Article:

Chen, W, Kemp, DB, He, T orcid.org/0000-0001-8975-8667 et al. (4 more authors) (2021) First record of the early Toarcian Oceanic Anoxic Event in the Hebrides Basin (UK) and implications for redox and weathering changes. Global and Planetary Change, 207. 103685. ISSN 0921-8181

https://doi.org/10.1016/j.gloplacha.2021.103685

First record of the early Toarcian oceanic anoxic event in the Hebrides Basin (UK) and implications for redox and weathering changes

Wenhan Chen [a], David B. Kemp [a*], Tianchen He [b], Chunju Huang [a], Simin Jin [a], Yijun Xiong [b], Robert J. Newton [b]

[a] State Key Laboratory of Biogeology and Environmental Geology, School of Earth Sciences, China University of Geosciences, Wuhan 430074, P.R. China
[b] School of Earth and Environment, University of Leeds, Leeds LS2 9JT, UK

*Corresponding author: David B. Kemp (davidkemp@cug.edu.cn)

Abstract

The early Toarcian (~183 Ma) was characterized by a prominent volcanism-induced warming event associated with a massive addition of ^{12}C-enriched carbon to the ocean-atmosphere system. This warming likely contributed to marked ocean deoxygenation during this time, giving the event its name: the early Toarcian oceanic anoxic event (T-OAE). Although the T-OAE has been recognized globally, clear geographic differences in the character of the event and its environmental effects have been noted. Here we present new carbon isotope, element abundance and organic geochemical data from a lower Toarcian succession on the Isle of Raasay, Scotland (Hebrides Basin, Northwest European Shelf). These data provide the first evidence of the T-OAE in Scotland. The succession is generally enriched in organic matter through the T-OAE interval, though redox-sensitive trace element data indicate that oxic-suboxic bottom water conditions prevailed, potentially interspersed with ephemeral anoxic episodes. Our elemental data contrast with evidence for persistent anoxia/euxinia in nearby basins, and emphasizes how deoxygenation was spatially variable and dependent on water depth and basin hydrography. Similarly, the data emphasize how anoxia was not a prerequisite for the deposition of organic-rich lithologies during the T-OAE. Sedimentological evidence, coupled with inorganic geochemical data, indicates increased coarse-grained detrital flux and enhanced chemical weathering during the T-OAE. Our findings support emerging evidence for a

marked strengthening of hydrological cycling and increased storminess at tropical and subtropical latitudes globally in response to global warming during the T-OAE.

1. Introduction

The early Toarcian oceanic anoxic event (T-OAE, ~183 Ma) (Jenkyns, 1988) was one of the most significant paleoenvironmental change events of the Phanerozoic. The interval was characterized by extinction of marine organisms (Harries and Little, 1999), floral turnover on land (Slater et al., 2019), and elevated seawater temperatures (Bailey et al., 2003; Ruebsam et al., 2020). A crisis in carbonate production also occurred (e.g. Han et al., 2018), putatively associated with ocean acidification (Suan et al., 2008; Ettinger et al., 2021). The event was also associated with a prominent sea-level rise (Hesselbo, 2008; Thibaut et al., 2018), widespread deposition of organic-rich sediments (Jenkyns, 1988), enhanced continental weathering (Cohen, et al., 2004; Them, et al., 2017; Kemp et al., 2020), and increased storm activity (Krencker et al., 2015; Han et al., 2018; Izumi et al., 2018a). Of particular significance is a pronounced negative carbon isotope excursion (CIE) recorded in marine organic carbon (Hesselbo et al., 2000), terrestrial organic carbon and fossil wood (Hesselbo et al., 2000; Xu et al., 2017), hemipelagic and shallow-water carbonates (Hesselbo et al., 2007; Han et al., 2018), and individual organic biomarkers (e.g. Schouten et al., 2000).

The CIE is interpreted to reflect a substantial injection of ^{12}C-enriched carbon into the ocean-atmosphere system, potentially caused by volcanism from the Karoo-Ferrar Large Igneous Province, the thermogenic emission of ^{12}C via intrusion of Karoo-Ferrar sills in Gondwanan coal deposits (McElwain et al., 2005; Svensen et al., 2007), and/or the dissociation of methane gas hydrates (Hesselbo et al., 2000, 2007; Kemp et al., 2005). The CIE is commonly broadly coeval with the deposition of organic-rich rocks, and the deposition of these facies worldwide has been linked to a significant episode of seawater deoxygenation (Jenkyns, 1988; Pearce et al., 2008). Nevertheless, the extent of seawater deoxygenation during the T-OAE is debated, and redox conditions appear to have been highly variable between different basins, water depths and oceans worldwide (e.g. Remirez and Algeo, 2020a). Given the fact that the oceanic environment has profound influences on extinction and radiation, it is important to dissect the reasons for this spatial variability in redox. Moreover, research on paleoclimate conditions during the T-OAE is of key importance for understanding the Earth system responses to large-scale carbon release, and necessitates global analysis from a range of geographic settings and environments.

In this paper, we present the first carbon isotope record of the T-OAE from the Hebrides Basin, deposited in the sub-Boreal realm (Figs. 1 and 2). Our dataset comprises bulk organic carbon isotope ($\delta^{13}C_{org}$), palynological carbon isotope ($\delta^{13}C_{paly}$), total organic carbon (TOC), Rock Eval pyrolysis, and element abundance data from a lower Toarcian succession on the Isle of Raasay, Scotland. Our results reveal the negative CIE in the sub-Boreal realm during the early Toarcian, which is coeval with deposition of organic-rich dark grey-black shales. Our new geochemical data permit a detailed investigation of seawater redox conditions through the T-OAE in the Hebrides Basin, and also provide insights into continental weathering and hydrological cycling in the sub-Boreal realm in response to T-OAE warming.

2. Geological setting

The Jurassic rocks of the Hebrides Basin are exposed in westerly-tilted fault blocks in a major half-graben (Fig. 2). The Hebrides Basin is one of a series of basins on the margins of the North Atlantic formed during early extensional phases in the evolution of the Central and North Atlantic Oceans (Tankard and Balkwill, 1989). The western margin of the Hebrides Basin is constrained by the Minch Fault Zone, east of the Outer Hebrides (Stein, 1988). The unfaulted eastern margin is adjacent to the present coastline of mainland Scotland (Morton and Hudson, 1995). Three phases of subsidence related to extension (Late Triassic to Early Toarcian, Latest Toarcian to Late Bathonian, and Early Oxfordian to Early Kimmeridgian) were separated by episodes of tectonic quiescence (Toarcian and Callovian) (Morton, 1989).

Successions spanning the upper Pliensbachian to lower Toarcian are exposed on the Isles of Skye and Raasay (Fig. 2; see, for example, Morton and Hudson, 1995). For this study, Toarcian samples were collected from Raasay, and are augmented by two samples collected from just below the Pliensbachian-Toarcian boundary on Skye (Figs. 2 and 3). Both localities were situated at a paleolatitude of ~40°N, close to the Viking corridor, which connected the Boreal Sea to northwestern Europe (Fig. 1).

2.1 Lithostratigraphy and depositional environment

The Toarcian succession on Raasay is exposed in and around disused ironstone mine workings at Inverarish Burn in the south of the island (UK Grid Reference NG 573365; Figs. 2 and 3). Here, the section (in ascending stratigraphic order) consists of a ~6 m succession of fine-grained sandstones of the uppermost Scalpa Sandstone Formation, dark grey-black micaceous shales of the Portree Shale Formation, and oolitic ironstones of the Raasay Ironstone Formation (Figs. 3 and 4; Lee, 1920; Howarth, 1956, 1992). The top of the Scalpa Sandstone Formation and fairly sharp transition to the darker and finer-grained Portree Shale Formation are exposed in a tributary to the northeast of the main ironstone workings (NG 5719 3688; Figs. 3B and 3C). The transition from the Portree Shale Formation to the Raasay Ironstone Formation is marked by dark grey-black shales with scattered chamosite ooids (Morton and Hudson, 1995), and can be observed on the floor of the opencast workings (NG 5690 3645). Nearby, numerous randomly oriented belemnites occur on a bedding surface (the "belemnite battlefield"), representing the top of the Portree Shale Formation (Fig. 3D; Doyle and Macdonald, 1993; Price, 2010). An abundant ammonite fauna in the Portree Shale Formation (Howarth, 1992) indicates deposition in a marine environment. A lack of observed sedimentary structures observed within this formation potentially indicates deposition in a quiescent environment. The transition from the Scalpa Sandstone Formation to the finer-grained Portree Shale Formation likely resulted from a relative sea-level rise (e.g. Morton, 1989).

The Raasay Ironstone Formation is characterized by thin, unevenly bedded chamosite oolitic ironstones, intercalated with thin argillaceous beds (Morton and Hudson, 1995; Figs. 3E and 3F). Previous work has indicated that some levels display cross-bedding, ostensibly suggesting that the ironstones formed in a shallow water environment with current action (Fig. 3F; Morton and Hudson, 1995). Hesselbo (2008) suggested that the ironstone represents an interval of sediment starvation during a sea level highstand. The samples collected from just below the Pliensbachian-Toarcian boundary on the Isle of Skye are from near the top of the Scalpa Sandstone Formation from a section exposed on the east coast of the island (NG 5156 4710; Figs. 2 and 3A).

2.2 Biostratigraphy

The *Dactylioceras tenuicostatum* Zone, marked by the first occurrence of the ammonite genus *Dactylioceras*, indicates the base of the Toarcian stage (Lee, 1920; Howarth, 1956, 1992). Poorly preserved *Dactylioceras tenuicostatum* fossils occur within the top 2 m of the Scalpa Sandstone Formation on Skye and Raasay, indicating that the base of the Toarcian is within this formation, and the *tenuicostatum* Zone extends into the lowest part of the overlying Portree Shale Formation (Howarth, 1992; Fig. 4). Above this, the *Harpoceras falciferum* Zone (equivalent to the *Harpoceras serpentinum* Zone) occurs within the rest of the Portree Shale Formation and overlying Raasay Ironstone Formation. The *falciferum* Zone can be subdivided into the *Cleviceras exaratum* and *Harpoceras falciferum* subzones. The *exaratum* Subzone in the Portree Shale Formation has been defined on the basis of the recognition of *Cleviceras exaratum*, coincident with the occurrence of dark grey-black shales (Lee, 1920; Howarth, 1992). The Raasay Ironstone Formation was assigned by Howarth (1992) to the *falciferum* Subzone and includes part of the *exaratum* Subzone based on the occurrence of *Cleviceras elegans* in the ironstone (Fig. 4). Importantly, previous studies (e.g. Lee, 1920; Price, 2010) erroneously assigned the Raasay Ironstone Formation to the *Hildoceras bifrons* Zone based on the purported presence of *Dactylioceras commune*. However, work by Howarth (1992) did not identify this species, and the presence of *Cleviceras elegans* confirms instead an (upper) *exaratum* Subzone age. All other species found in the Raasay Ironstone Formation indicate a *falciferum* Subzone age (Howarth, 1992), and thus the Raasay Ironstone Formation must span at least the upper part of the *exaratum* Subzone and an unknown proportion of the *falciferum* Subzone (Howarth, 1992; Fig. 4).

3. Materials and methods

3.1 Sample collection

At Inverarish Burn, 20 rock samples were collected from the upper part of the Portree Shale Formation and Raasay Ironstone Formation from the main opencast workings (NG 5690 3645) at approximately 15 cm intervals. Thirty-eight samples were also obtained from the uppermost Scalpa Sandstone Formation and Portree Shale Formation from the tributary northeast of the main opencast workings (NG 5719 3688) at intervals of 10 cm or less. Based on the orientation of the bedding in this area, an exposure gap of ~13 cm separates the two sample sets (Fig. 4). On Skye, 2 samples were collected from the uppermost Scalpa Sandstone Formation from the highest exposed and accessible outcrop (NG 5156 4710; Figs. 2 and 3A). According to the litho- and biostratigraphy of Morton (2009), these samples are from the *P. hawskerense* Subzone of the *Pleuroceras spinatum* Zone (Pliensbachian stage) (Fig. 4).

3.2 Carbon isotopes, TOC, and nitrogen abundance

All 60 samples were analyzed for bulk organic carbon isotope ratios ($\delta^{13}C_{org}$), total organic carbon (TOC), and nitrogen abundance at the State Key Laboratory of Geological Processes and Mineral Resources, China University of Geosciences (Wuhan). For each sample, approximately 1g of powdered rock was reacted with 20% HCl for at least 24 hours to remove carbonate phases. Samples were then repeatedly washed with distilled water to remove residual acid. After drying, around 50 mg of each sample powder was sealed in Sn foil for isotope analyses through a Thermo Finnigan MAT 253 mass spectrometer, which yielded an instrumental precision (standard deviation) of 0.1‰. Standard samples GBW04407 (-22.43‰ ± 0.07) and GBW04408 (-36.91‰ ± 0.10) were used for the calibration, and the results are reported relative to the Vienna Pee Dee Belemnite (VPDB) standard. TOC and N abundance analyses were conducted on samples using a Vario MACRO cube elemental analyzer. Phenylalanine was used as the calibration standard and the analytical precision for C and N was better than 0.2 wt.%. Additionally, 22 samples spread evenly through the succession were analyzed for palynological carbon isotope composition ($\delta^{13}C_{paly}$). This analysis was carried out to specifically test the veracity of the bulk organic matter $\delta^{13}C$ analyses, since the likely presence of siderite in the Raasay Ironstone (Morton, 2009) could lead to recalcitrant carbonate carbon resistant to decalcification using dilute HCl. For this process, ~1g of powdered sample was reacted with concentrated HCl and HF, before the addition of zinc bromide to remove residual mineral grains. The organic matter residue was then measured using a MAT 253 mass spectrometer, with a precision (standard deviation) obtained from standards (USGS 40, USGS 41A, QUB) of ≤0.13‰.

3.3 Rock Eval pyrolysis

Rock Eval pyrolysis generates hydrogen index (HI, mg hydrocarbons/g TOC), oxygen index (OI, mg CO_2/g TOC) and T_{max} (°C) data, which can be useful for understanding the type and maturity of organic matter (Espitalié et al., 1985). Organic matter pyrolysis of 11 whole-rock powdered samples spread through the Raasay section was conducted at the Guangzhou Institute of Geochemistry, Chinese Academy of Sciences using a Rock Eval 6 instrument, following the method described in Espitalié et al. (1985). The IFP 160000 standard was used to calibrate results.

3.4 Elemental analysis

Thirty-five powdered samples were analyzed for element abundances. Twenty-two of them were analyzed at the University of Leeds. For these samples, 80mg of powdered sample was dissolved in a HNO_3-HF-$HClO_4$ mixture, followed by evaporation to dryness. Boric acid was then added to the residue, before achieving total dissolution with hot HNO_3. Major and trace elements were measured by ICP-OES and ICP-MS with multiple replicate analyses of one sample yielding relative standard deviations (RSDs) of <2%. The other 13 samples were sent to Nanjing FocuMS Technology Co. Ltd, because they were difficult to fully digest with the above method. For these samples, about 40 mg of powdered sample was mixed with HNO_3 and HF in high-pressure PTFE bombs. These bombs were then placed in an oven at 195℃ for at least 48 hours to ensure digestion, after which the digested diluent was nebulized into an Agilent Technologies 7700x quadrupole ICP-MS to determine the major and trace elements. Multiple replicate analyses of one sample and standards yielded RSDs of <5%.

4. Results

4.1 Carbon isotopes, TOC and TOC/N

Bulk organic carbon isotope ($\delta^{13}C_{org}$), palynological carbon isotope ($\delta^{13}C_{paly}$), and TOC data are plotted against the stratigraphy in Fig. 4 (data available in Table S1). The $\delta^{13}C_{org}$ values in the Raasay section range from −27.17‰ to −24.49‰, and show a decrease of ~2.7‰ upwards through the studied section. This overall decrease in $\delta^{13}C_{org}$ comprises three abrupt negative shifts (each <30 cm thick) between the uppermost Scalpa Sandstone Formation (*tenuicostatum* Zone), and the base of the Raasay Ironstone Formation (*exaratum* Subzone). This is followed by a plateau and a slight recovery (i.e. positive trend in $\delta^{13}C_{org}$) to the top of the Raasay Ironstone Formation. The variations of paired $\delta^{13}C_{paly}$ values show a similar trend and match well with $\delta^{13}C_{org}$ measured on the same samples. The two samples collected from Skye in the Scalpa Sandstone Formation below the Pliensbachian-Toarcian boundary (*spinatum* Zone) show relatively high $\delta^{13}C_{org}$ values (-24.80‰ and -24.58‰) that are similar to those of the uppermost Scalpa Sandstone Formation at the base of the Raasay section.

In detail, the onset of the first negative shift (shift 1) is at -40 cm section height in the Raasay section, and spans ~20 cm of the *tenuicostatum* Zone in the Scalpa Sandstone Formation with a magnitude of ~1.0‰. Subsequently, values are broadly stable before the second abrupt shift (shift 2) of ~1.0‰ at 140 cm in the Portree Shale Formation, which spans ~30 cm. The third abrupt negative shift (shift 3, ~1.1‰) occurs ~120 cm above the top of shift 2 (~290 cm section height), and is characterized by a sharp decrease to minimum $\delta^{13}C_{org}$ (-27.07‰) over ~20 cm in the lower part of the Raasay Ironstone Formation (*exaratum* Subzone). Through the rest of the Raasay Ironstone Formation, $\delta^{13}C_{org}$ is broadly stable but with a slight increasing trend of ~1.3‰.

TOC values in the Raasay section range from 0.24% to 8.01% (mean 2.05%), and TOC in the two Skye samples is 0.04% and 0.05% (Fig. 4). TOC gradually increases from 0.55% at the base of the Raasay section to 3.27% at 155 cm in the Portree Shale Formation. Following a decline to 1.03% in the lowermost Raasay Ironstone Formation (260 cm), TOC rises abruptly to the highest value (8.01%) at 355 cm in the Raasay Ironstone Formation. This is close to the level where minimum $\delta^{13}C_{org}$ occurs. Above this, TOC values show an overall decrease towards the top of the succession. TOC/N ratios in the Raasay section range from ~8 to ~29, with a mean of ~20 (Fig. 5). A pronounced increase to ~29 occurs from the lower part of the Portree Shale Formation through to the Raasay Ironstone Formation, followed by a drop to ~11 towards the top of the section (Fig. 5; Table S1).

4.2 Rock Eval pyrolysis

Hydrogen index (HI) values range between 16 and 168 (mean 48 mg HC/g TOC), and are relatively steady throughout the succession, with the highest value recorded within the Raasay Ironstone Formation (Figs. 5 and 6). Oxygen index (OI) values range between 5 and 67 (mean 22 mg CO_2/g TOC, Figs. 5 and 6). T_{max} is also broadly stable, ranging from 337℃ to 426℃ with no abrupt fluctuations, except an outlying value (583℃) within the Portree Shale Formation (Fig. 5; Table S1).

4.3 Elemental abundances

4.31 Redox-sensitive elements

Mo, U, V, and Re have long been used to assess paleoredox conditions, and the relative enrichment of Ni can be a useful indicator of primary productivity (e.g. Tribovillard et al., 2006, 2012; Algeo and Tribovillard, 2009; Liu et al., 2021). In this study, enrichment factors (EFs) have been used to describe and assess the abundance of these elements relative to average shale values (Fig. 7). Enrichment factors are calculated as $X_{EF} = (X/Al)_{sample}/(X/Al)_{PAAS}$, where PAAS refers to post-Archean average Australian shale (from Taylor and McLennan, 1985). If X_{EF} is greater than 1, then element X is enriched relative to the average shale, otherwise it is depleted. In practical terms, an X_{EF} >3 can be regarded as detectably enriched, and an X_{EF} >10 is substantially enriched (Algeo and Tribovillard, 2009).

In general, Mo_{EF} is <1 from the base of the Raasay section up to ~310 cm in the Raasay Ironstone Formation. Above this level, Mo_{EF} increases to >1, reaching a maximum (~8) at 494 cm in the Raasay Ironstone Formation (Fig. 7). Mean Mo_{EF} in the succession is ~1.13. From the base of the succession to ~100 cm, U_{EF} values are generally <3. Above this level, there are some fluctuations and a marked increase (up to ~113) at 193 cm in the Portree Shale Formation. Values then decrease to ~12 at 213 cm and remain steady (~7) until 370 cm section height, followed by a marked rise (up to ~27) to the top of the succession through the Raasay Ironstone Formation (Fig. 7). Mean U_{EF} in the succession is ~12.41. V_{EF} ranges between ~1 and ~11 (mean ~3.61) throughout the succession. Overall, V_{EF} rises progressively from the base of the succession to ~3 at 370 cm in the Raasay Ironstone Formation, before increasing more abruptly to ~10 at 406 cm and remaining high above this (Fig. 7). Ni_{EF} values are low and generally stable (~1) from the base of the succession to ~100 cm. Subsequently, Ni_{EF} increases to ~3 at ~180 cm in the upper Portree Shale Formation, followed by a marked decrease to ~1 at ~300 cm. Higher in the section, Ni_{EF} rises again (up to ~8) within the Raasay Ironstone Formation and remains high at the top of the succession (Fig. 7).

Ratios of Mo_{EF}/U_{EF} and V_{EF}/Mo_{EF} show obvious negative correlation throughout the succession (Fig. 7). Two intervals, characterized by generally increasing Mo_{EF}/U_{EF} and decreasing V_{EF}/Mo_{EF}, can be observed in the shaded intervals of Fig. 7 (labelled intervals A and B) and contrast with the overall decreasing trends in Mo_{EF}/U_{EF} in the rest of the section. Re/Mo values show a prominent rise from ~35 at the base of the succession to ~193 at ~110 cm, followed by a sharp decrease to ~21 at ~180 cm in the Portree Shale Formation. Above this, values increase to ~116 and are relatively high (~105) from ~190 to ~250 cm, after which values fall sharply up-section, and are close to 0 at the top of the succession (Fig. 7).

4.32 Detrital and chemical weathering proxies

Variations in the flux and nature of detrital components can be tracked using elements that are typically enriched in terrigenous sediments. Proxies for variations in detrital flux and grain size (Ti/Al, Ti/K and Zr/Rb) show similar trends with differing magnitudes through the section (Fig. 8). These proxies are generally relatively low and stable from the base of the section to ~80 cm. Subsequently, there is a prominent rise in Ti/K and Zr/Rb to the top of the Portree Shale Formation (Fig. 8, note logarithmic scales), and a smaller magnitude rise in Ti/Al. Ti/Al, Ti/K and Zr/Rb values increase abruptly near the base of the Raasay Ironstone Formation (Fig. 8). Chemical weathering proxies (K/Al and Rb/Al) show some fluctuations from the base of the section to ~20 cm. Above this, K/Al and Rb/Al drop sharply to ~100 cm, followed by a plateau to ~250 cm near the base of the Raasay Ironstone Formation. Further up-section, values decrease again to ~360 cm, and remain low to the top of the section (Fig. 8).

5. Discussion

5.1 The Toarcian OAE and CIE in the Hebrides Basin

The available ammonite age constraints for the Raasay succession (Section 2.2) indicate an early Toarcian age that is contemporaneous with the Toarcian OAE recognized globally. As such, the ~2.7‰ decrease in $\delta^{13}C_{org}$ through the uppermost Scalpa Sandstone Formation (*tenuicostatum* Zone), Portree Shale Formation (*exaratum* Subzone), and the lowermost Raasay Ironstone Formation (*exaratum* Subzone) can be unambiguously correlated with the fall in $\delta^{13}C_{org}$ recognized from the same ammonite zones in other basins. Specifically, our new $\delta^{13}C_{org}$ data can be correlated with the well-studied and nearby Yorkshire section from the Cleveland Basin (Figs. 1B and 9). Within the constraints of the available ammonite biostratigraphy from both sites, the 3 abrupt negative $\delta^{13}C_{org}$ shifts observed on Raasay may correlate with 3 similar abrupt shifts recognized in Yorkshire (Fig. 9; Kemp et al., 2005). In the Yorkshire section, the shifts are more abrupt (<10 cm each) and more closely spaced than on Raasay (Fig. 9). A similar pattern of 2 or 3 shifts within the decreasing part of the T-OAE CIE has been recognized elsewhere (see for example Xu et al., 2018 and Izumi et al., 2018a). This correlation implies that the Raasay section (which does not capture the CIE in its entirety) may be stratigraphically expanded relative to Yorkshire. Nevertheless, the veracity of the correlation is difficult to confirm owing to the lack of additional independent time constraints in the Raasay section (Fig. 9).

One important difference between the Raasay $\delta^{13}C_{org}$ data and those of the nearest high-resolution $\delta^{13}C_{org}$ record in Yorkshire is that the magnitudes of the negative shifts are smaller on Raasay (Fig. 9). In the Yorkshire succession, the overall decrease in bulk $\delta^{13}C_{org}$ from the *tenuicostatum* Zone to *exaratum* Subzone is ~7‰, and each negative shift is ~2‰ or larger (Fig. 9). In other nearby basins in Europe, the magnitude of the T-OAE CIE also tends to be greater than we observe on Raasay, with more negative background (i.e. pre-excursion) values (see Remirez and Algeo, 2020a for a review). Globally, the magnitude of the CIE is variable (e.g. Remirez and Algeo, 2020a), and the CIE magnitude we observe on Raasay is consistent with $\delta^{13}C_{org}$ data from a number of sections globally, including Switzerland (Fantasia et al., 2018), Canada (Them et al., 2017), Japan (Ikeda et al., 2018) and Tibet (Han et al., 2018).

Thermal maturity and variations in organic matter (OM) sources can have a potentially large impact on bulk organic carbon isotopes (e.g. Suan et al., 2015; Kemp et al., 2019). Rock Eval pyrolysis metrics, specifically HI, OI and T_{max}, can be used to track OM sources and assess thermal maturity (van Krevelen, 1981; Espitalié et al., 1985). Kerogens can be classified into four types (I–IV) based on different OM sources. In detail, algal and marine-derived OM (kerogen Type I and II) is hydrogen-rich with correspondingly high HI values. Type III primarily derives from terrestrial higher plants with relatively depleted hydrogen content, while type IV commonly consists of inertinite of terrestrial origin that is oxidized/reworked with extremely low HI values. T_{max} is an indicator of thermal maturity. As shown in Figs. 5 and 6, low HI values (16 to 168 mg, mean 48 HC/g TOC) and OI values (5 to 67 mg, mean 22 mg CO_2/g TOC) characterize the Raasay section, likely indicating a mix of terrestrially derived Type III and Type IV OM. In spite of an outlier (583℃) at 170 cm, T_{max} values are generally low (below 430℃). This observation suggests little post-depositional diagenetic alteration of the organic matter or elemental data presented. Overall, the data suggest the predominance of relatively immature organic matter with negligible thermal alteration that could otherwise affect the $\delta^{13}C_{org}$ signal or our other data.

In addition to Rock Eval, TOC/N can be used as a supplementary proxy to assess organic matter source. Vascular land plants typically have TOC/N >20, whereas algal organic matter of marine origin generally has TOC/N <10 (e.g. Meyers, 1997). Mean TOC/N in the Raasay section is ~20, and the values increase during the T-OAE (Fig. 5), likely reflective of a predominance of terrestrial organic matter in this interval. The reliability of using TOC/N in this way has been questioned (e.g. Wang et al., 2021), but the results obtained are consistent with the Rock Eval data in that they indicate a predominantly terrestrial source of organic matter. In detail, there is a weak trend in TOC/N that broadly mirrors the shape of the CIE on Raasay (Fig. 5; Fig S1A). However, the correlation between $\delta^{13}C_{org}$ and TOC/N is relatively weak (R^2 ~0.17). As such, any changes in organic matter source through the section likely had only a minor impact on the magnitude and morphology of the CIE. Similarly, the good match between the measured $\delta^{13}C_{paly}$ values and the bulk $\delta^{13}C_{org}$ data (R^2 ~0.82; Fig. S1B) suggests that incomplete decalcification of refractory carbonate carbon is also unlikely to explain the lower magnitude change in $\delta^{13}C_{org}$ and higher overall values in the Raasay section relative to nearby basins.

Suan et al. (2015) showed that the magnitude of the Toarcian CIE in a number of sections, including Yorkshire, is amplified by changing organic matter source through the excursion. They suggested a more realistic global magnitude of ~3-4‰ for the CIE (3.2‰ in Yorkshire). This is close to the magnitude observed in the Raasay section (Suan et al., 2015).

5.2 Redox conditions in the Hebrides Basin during the T-OAE

Mean TOC in the Raasay section is ~2.0%, and the progressive increase in TOC (up to ~8.01%) in the lower part of the Raasay Ironstone Formation may suggest the development of oxygen-deficient bottom water conditions. Our RSTE (redox-sensitive trace element) data can help discriminate between different seawater redox conditions, generally classified as oxic (>2.0 ml O_2 L^{-1}), suboxic (~0.2-2.0 ml O_2 L^{-1}), anoxic–nonsulfidic (<0.2 ml O_2 L^{-1}, 0 ml H_2S L^{-1}), and euxinic (0 ml O_2 L^{-1}, >0ml H_2S L^{-1}) (Wignall, 1994).

Mo, U and V accumulate strongly under reducing conditions. In some modern marine systems characterized by intense Mn-Fe redox cycling within the water column (e.g. Cariaco Basin), the accumulation of authigenic Mo in sediments will be strengthened via a "particulate shuttle" (Algeo and Tribovillard, 2009). In highly restricted settings, the resupply of dissolved Mo available for enrichment in sediments may be limited, resulting in a low Mo abundance and low Mo/TOC even under euxinic conditions (Algeo and Lyons, 2006; McArthur et al., 2008). The possible spread of anoxic/euxinic conditions worldwide during the OAE (e.g. Dickson, 2017) could have caused a global seawater Mo drawdown, leading to a universal decrease in Mo concentration even in organic-rich sediments (e.g. Algeo, 2004; Goldberg et al., 2016). The reduction of U starts at the Fe (II)–Fe (III) redox boundary and links directly with Fe redox reactions rather than the presence of free H_2S in the water column (euxinia) (Algeo and Maynard, 2004). Consequently, enrichment of U takes place under less intensely reducing conditions compared to Mo. V is much more sensitive to redox variation and tends to be well preserved after burial with little reworking or remobilization (Algeo, 2004). Therefore, the enrichment of V in sediments can be a useful tracer for weakly reducing (suboxic) or oscillating redox conditions (Calvert and Pedersen, 1993). Variations in Mo_{EF}/U_{EF} and V_{EF}/Mo_{EF} ratios are useful for monitoring relative enrichment among these redox-sensitive elements, providing additional indications for the degree of deoxygenation in bottom waters (e.g. Scholz, 2018). Similarly, Re is conservative in seawater under oxic settings, and accumulates strongly under suboxic conditions in particular (Crusius et al., 1996). Because Mo accumulation tends to be strengthened under euxinic conditions, Re/Mo can thus be employed to discriminate between suboxic and euxinic conditions.

In the Raasay section, Mo is typically depleted relative to PAAS values (Fig. 7). Mo/TOC ratios are extremely low during the negative trend in $\delta^{13}C_{org}$, and similar to values recorded across the T-OAE in the Yorkshire and Sakuraguchi-dani sections (Cleveland and Tabe Basins, respectively; Fig. 10). Low Mo and Mo/TOC ratios in the Cleveland Basin reflect extreme hydrographic restriction and persistent euxinia during the T-OAE (McArthur et al., 2008; Remirez and Algeo, 2020b). By contrast, low Mo and Mo/TOC in the Tabe Basin and lack of strong enrichment in other redox elements indicate the predominance of oxic to suboxic bottom water conditions (Kemp and Izumi, 2014), perhaps with intermittent anoxia/euxinia based on limited pyrite framboid evidence (Izumi et al., 2018b). Therefore, two scenarios could be proposed to explain the low Mo_{EF} and Mo/TOC ratios observed in the Raasay section. In the first scenario, the Hebrides Basin became restricted like the Cleveland Basin with an anoxic environment from the onset of the negative trend in $\delta^{13}C_{org}$, during which inadequate replenishment of Mo led to both low Mo_{EF} and Mo/TOC values. The increase in Mo_{EF} within the Raasay Ironstone Formation could indicate a more open environment in the Hebrides Basin at this time, and consequent resupply of Mo, possibly supported by a global sea level rise during the interval (Hesselbo, 2008). The alternative scenario is that low Mo and Mo/TOC ratios simply reflect a predominantly oxic to suboxic environment within an unrestricted setting. In this case, the high TOC (which is predominantly terrestrial in origin based on the Rock Eval and TOC/N data) could have resulted primarily from high input of terrestrial material, with preservation potentially aided by relatively high sedimentation rates and/or suboxic conditions at the sea floor.

Persistent anoxic or euxinic conditions through the T-OAE on Raasay are unlikely owing to the lack of strong evidence in the other redox data and the paleoecology of the section (Fig. 7). U and V are only moderately enriched through the succession, suggesting suboxic conditions. Ni_{EF} is a useful proxy to assess organic carbon flux related to primary productivity, as well as redox conditions (Tribovillard et al., 2006), and on Raasay Ni_{EF} values are generally <3. Paleontological data from NW Europe indicate that four bivalve species commonly dominate the lower Toarcian: *Bositra radiata*, *Pseudomytiloides dubius*, *Meleagrinella substriata*, and *Bositra buchi* (Little, 1995). Facies containing primarily *Meleagrinella* and *Bositra* may indicate oxic-suboxic bottom water conditions, whereas *P. dubius* has been considered a low-oxygen specialist, i.e. the most tolerant or well adapted species (Little, 1995; Caswell et al., 2009). *Meleagrinella substriata*, *Liostrea hisingeri*, and *Propeamussium pumilum* occur in the Portree Shale Formation and Raasay Ironstone Formation, and *P. dubius* is not recorded. Thus, combined with the presence of low-oxygen intolerant taxa like *Chariocrinus wuerttembergicus* and *Orthotoma sp. A* in the Raasay Ironstone

Formation (Little, 1995), the Hebrides Basin can be interpreted as suboxic-oxic during the T-OAE, consistent with our redox-sensitive element data. Anoxia was not a prerequisite for the deposition of organic-rich lithologies during the T-OAE, as also found at other sites (e.g. Kemp and Izumi, 2014).

Interestingly, there is a prominent decline in Re/Mo and V_{EF}/Mo_{EF}, concurrent with an increase in U_{EF}, V_{EF}, Ni_{EF} and Mo_{EF}/U_{EF}, from ~110 to ~180 cm in the Portree Shale Formation (the shaded interval A on Fig. 7), indicating the probable occurrence of anoxia during this interval. However, similar variations in Mo_{EF}/U_{EF} and V_{EF}/Mo_{EF} ratios from ~240 to ~370 cm (the shaded interval B on Fig. 7) in the Raasay Ironstone Formation instead may be interpreted as the preferred trapping of Mo by Fe oxides minerals via a particulate shuttle in an oxic-suboxic setting (e.g. Algeo and Tribovillard, 2009; Percival et al., 2016).

The interpretation of oxic-suboxic bottom-water conditions in the Hebrides Basin during the T-OAE contrasts with data from the nearby Cleveland Basin, as well as a number of other basins in northern Europe, where anoxia/euxinia was pervasive (e.g. McArthur et al., 2008). This finding helps to emphasize that the T-OAE was not characterized by a single and continuous anoxic interval on the Northwest European Shelf (NWES). A shallower water depth and/or unrestricted setting at the Raasay site could be key reasons for this. Equally, ocean-atmosphere models of the Toarcian (Dera and Donnadieu, 2012; Ruvalcaba Baroni et al., 2018) indicate that southward flow from the Arctic through the Viking Corridor might have been strengthened during the T-OAE. This current would have potentially delivered colder oxygenated waters into the NWES area and significantly influence the local redox conditions. Given its proximity to the Viking corridor (Fig. 1), the bottom water of the Hebrides Basin might have been kept oxygenated by this flow.

5.3 Detrital and chemical weathering signals in the Hebrides Basin during the T-OAE

Ti and Zr are typically enriched in coarse grained rocks like siltstones and sandstones owing to their presence in heavy minerals like rutile and zirconium, which are typically transported with coarse fraction sediments. By contrast, Al, Rb and K are typically relatively abundant in K-feldspar, mica and clay minerals (Calvert and Pedersen, 2007). Therefore, proxies such as Ti/Al, Zr/Rb and Ti/K (in combination with sedimentological observations) are useful for revealing variations in detrital fluxes in marine sediments (Calvert and Pedersen, 2007). At the same time, Rb and K in terrestrial sediments are also useful for inferring changes in weathering. Due to ionic size similarities between Rb and K, Rb can substitute for K in potassium feldspars (Calvert and Pedersen, 2007). K and Rb are sensitive to strong chemical weathering, resulting in K and Rb loss from sediments via leaching, leaving Al relatively enriched in clay mineral products. Consequently, K/Al and Rb/Al ratios can be utilized to reveal variations in continental chemical weathering.

On Raasay, Ti/K and Zr/Rb ratios show large-scale increases through the section, suggesting sediment coarsening (Fig. 8). At ~310 cm near the base of the Raasay Ironstone Formation, for instance, an increase of over two orders of magnitude is coincident with the change from shale to ironstone (Fig. 8). Nevertheless, we also observe that K/Al and Rb/Al ratios decrease synchronously up-section (Fig. 8) and broadly mirror the Ti/K and Zr/Rb data. The steady loss of K and Rb through this part of the succession, despite being clay-rich, suggests increasing chemical weathering in the sediment source area. Similarly, the near-total absence of K and Rb in the Raasay Ironstone above ~360 cm suggests intensified weathering. Given the likely influence of weathering on the relative abundance of K and Rb, a more robust proxy for grain-size changes in the section is Ti/Al. These data show a much subtler but steady rise through the Portree Shale Formation and lower part of the Raasay Ironstone Formation, indicative of coarsening (Fig. 8). A more marked increase in Ti/Al occurs at ~370 cm, indicating abrupt sediment coarsening coeval with minimum values in $\delta^{13}C_{org}$ (Fig. 8). Taken together, the data suggest an enhancement of continental chemical weathering through the T-OAE that is broadly coincident with a rise in coarse-grained terrigenous sediment input.

The occurrence of wavy-bedded and cross-bedded oolitic ironstones in the Raasay Ironstone Formation (see Section 2.1) ostensibly suggests a shallow marine depositional environment (Morton and Hudson, 1995). Because global sea level was rising through this interval (Hesselbo, 2008; Thibault et al., 2018), previous work has argued that the ironstones did not form *in situ*, and that instead the ooids were derived from shoals on nearby fault-bounded topographic highs, with the muddy layers representing the background sedimentation (Little, 1995). Hesselbo (2008) suggested that sea-level highstand during deposition of the Raasay Ironstone Formation may have led to sediment starvation that promoted ironstone formation. Importantly, however, it is now widely recognized that hydrological cycling intensified during the Toarcian OAE (e.g. Krencker et al., 2015; Izumi et al., 2018a; Han et al., 2018). If an increase in hydrological cycling occurred in the Hebrides Basin, this could have increased the frequency and/or magnitude of storm events and wave action, resulting in high energy conditions that winnowed fine-grained clastic material leaving behind denser, iron-rich coarse sediments (i.e. ooids, see for example Akande and Mücke, 1993). At the same time, intense chemical weathering on land could have leached reactive Fe, providing the source for ironstone formation. Strong current action can also explain the cross-bedding in the ironstone previously reported (Morton and Hudson, 1995).

The Raasay section was situated at a higher paleolatitude (~40°N) than the tropical locations where previous evidence of increased storminess has generally been found (Krencker et al., 2015; Han et al., 2018). Winter storms, normally generated at mid to high latitudes by air mass disturbances (i.e. mixing of warm air currents from the low latitudes and cold air currents from the polar areas; Masselink and van Heteren, 2014), may have been a cause of storms during deposition of the Raasay Ironstone Formation. On the other hand, intensified and more frequent tropical cyclones, associated with the known increase in atmospheric CO_2 and seawater temperature during the Toarcian OAE (McElwain et al., 2005; Bailey et al., 2003; Ruebsam et al., 2020), could have affected higher latitudes. Coupled ocean-atmosphere climate models have predicted significant enhancement of hydrological cycling as well as a poleward expansion of tropical summer storms as a consequence of rapid rises in $p$$CO_2$ and seawater temperature, both in the Toarcian and at the present day (Dera and Donnadieu, 2012; Emanuel, 2016; Korty et al., 2017). Storm activity in the Hebrides Basin may have prevented the development of a stable chemocline, further helping to maintain more oxygenated conditions relative to the nearby (and likely deeper) Cleveland Basin.

6. Conclusions

Sedimentological and geochemical analyses of a Toarcian section on the Isle of Raasay reveal the expression of the Toarcian Oceanic Anoxic Event in the Hebrides Basin for the first time. Organic carbon isotope data reveal a significant negative trend (~-2.7‰) during the early Toarcian, which is similar to the trend and pattern observed in contemporaneous carbon isotope data globally. Redox-sensitive trace element data, coupled with paleontological information, indicate oxygenated to suboxic conditions in the Hebrides Basin through the T-OAE. This contrasts with the strong anoxia and euxinia recorded in nearby basins, and can likely be attributed at least in part to water depth differences, the unrestricted nature of the basin, and proximity to the possible southward flow of cold oxygenated water through the Viking corridor. A significant strengthening of continental weathering through the T-OAE on Raasay is inferred from sediment coarsening and decreasing K/Al and Rb/Al ratios. In the context of the global warming known to have occurred during the event, we suggest that intensified hydrological cycling accelerated continental weathering and increased riverine transport capacity and coarse grain sediment delivery to the basin. High-energy conditions linked to storm activity may have further limited seawater deoxygenation in the basin.

Acknowledgements

This work was supported by the National Natural Science Foundation of China (Grant No. 41888101) to DBK and TH, and the National Recruitment Program for Young Professionals (P.R. China) to DBK. RN was funded by the Natural Environment Research Council (grant NE/N018559/1). This manuscript is a contribution to the Integrated Understanding of the Early Jurassic Earth System and Timescale (JET) project and IGCP 739. We thank Jinyoung Gil for help in the field and Sen Li, Yinggang Zhang for assistance in the lab. We are grateful to Zhixiang Wang and Dongyang Liu for the helpful discussion.

Appendix A. Supplementary material

Supplementary material related to this article can be found on-line at https://

References

Akande, S.O., Mücke, A., 1993. Depositional environment and diagenesis of carbonates at the Mamu/Nkporo Formation, Anambra basin, Southern Nigeria. Journal of African Earth Sciences 17 (4), 445–456.

Algeo, T.J., 2004. Can marine anoxic events draw down the trace element inventory of seawater? Geology 32, 1057–1060.

Algeo, T.J., Maynard, J.B., 2004. Trace-element behavior and redox facies in core shales of Upper Pennsylvanian Kansas-type cyclothems. Chem. Geol. 206, 289–318.

Algeo, T.J., Lyons, T.W., 2006. Mo-total organic carbon covariation in modern anoxic marine environments: implication for analysis of paleoredox and -hydrographic conditions. Paleoceanography 21, PA1016 23 pp.

Algeo, T.J., Tribovillard, N., 2009. Environmental analysis of paleoceanographic systems based on molybdenum–uranium covariation. Chem. Geol. 268 (3–4), 211–225.

Bailey, T.R., Rosenthal, Y., McArthur, J.M., van de Schootbrugge, B., Thirlwall, M.F., 2003. Paleoceanographic changes of the Late Pliensbachian–Early Toarcian interval: a possible link to the genesis of an Oceanic Anoxic Event. Earth Planet. Sci. Lett. 212 (3–4), 307–320.

Calvert, S.E., Pedersen, T.F., 1993. Geochemistry of Recent oxic and anoxic marine sediments: Implications for the geological record. Mar. Geol. 113, 67–88.

Calvert, S.E., Pedersen, T.F., 2007. Chapter Fourteen Elemental Proxies for Palaeoclimatic and Palaeoceanographic Variability in Marine Sediments: Interpretation and Application. Developments in Marine Geology 1 (4), 567–644.

Caswell, B.A., Coe, A.L., Cohen, A.S., 2009. New range data for marine invertebrate species across the early Toarcian (Early Jurassic) mass extinction. Journal of the Geological Society 166 (5), 859–872.

Cohen, A.S., Coe, A.L., Harding, S.M., Schwark, L., 2004. Osmium isotope evidence for the regulation of atmospheric CO2 by continental weathering. Geology 32 (2), 157–160.

Crusius, J., Calvert, S., Pedersen, T., Sage, D., 1996. Rhenium and molybdenum enrichments in sediments as indicators of oxic, suboxic and sulfidic conditions of deposition. Earth Planet. Sci. Lett. 145, 65–78.

Dera, G., Pellenard, P., Neige, P., Deconinck, J.F., Pucéat, E., Dommergues, J.-L., 2009. Distribution of clay minerals in Early Jurassic Peritethyan seas: palaeoclimatic significance inferred from multiproxy comparisons. Palaeogeogr. Palaeoclimatol. Palaeoecol. 271, 39–51.

Dera, G., Donnadieu, Y., 2012. Modeling evidences for global warming, Arctic

seawater freshening, and sluggish oceanic circulation during the Early Toarcian anoxic event. Paleoceanography 27, 1–15.
Dickson, A.J., 2017. A molybdenum-isotope perspective on Phanerozoic deoxygenation events. Nat. Geosci. 10, 721–726.Espitalié, J., Deroo, G., Marquis, F., 1985. La pyrolyse Rock-Eval et ses applications. Deuxieme partie. Revue de l'Institut francais du Petrole 40 (6), 755–784.
Doyle, P., Macdonald, D.I.M., 1993. Belemnite battlefields. Lethaia 26, 65–80.
Emanuel, K.A., 2016. Will global warming make hurricane forecasting more difficult? Bull. Am. Meteorol. Soc. 98 (3), 495–501.
Ettinger, N.P., Larson, T.E., Kerans, C., Thibodeau, A.M., Hattori, K.E., Kacur, S.M., Martindale, R.C., 2021. Ocean acidification and photic-zone anoxia at the Toarcian Oceanic Anoxic Event: Insights from the Adriatic Carbonate Platform. Sedimentology 68 (1), 63–107.
Fantasia, A., Follmi, K.B., Adatte, T., Spangenberg, J.E., Montero-Serrano, J.C., 2018. The Early Toarcian oceanic anoxic event: Paleoenvironmental and paleoclimatic change across the Alpine Tethys (Switzerland). Glob. Planet. Chang. 162, 53–68.
Goldberg, T., Poulton, S.W., Wagner, T., Kolonic, S.F., Rehkämper, M., 2016. Molybdenum drawdown during Cretaceous Oceanic Anoxic Event 2. Earth Planet. Sci. Lett. 440, 81–91.
Han, Z., Hu, X., Kemp, D.B., Li, J., 2018. Carbonate-platform response to the Toarcian Oceanic Anoxic Event in the southern hemisphere: Implications for climatic change and biotic platform demise. Earth Planet. Sci. Lett. 489, 59–71.
Harries, P.J., Little, C.T.S., 1999. The early Toarcian (Early Jurassic) and the Cenomanian-Turonian (Late Cretaceous) mass extinctions: similarities and contrasts. Palaeogeogr. Palaeoclimatol. Palaeoecol. 154, 39–66.
Hesselbo, S.P., Grocke, D.R., Jenkyns, H.C., Bjerrum, C.J., Farrimond, P., Bell, H.S.M., Green, O.R., 2000. Massive dissociation of gas hydrate during a Jurassic oceanic anoxic event. Nature 406 (6794), 392–395.
Hesselbo, S.P., Jenkyns, H.C., Duarte, L.V., Oliveira, L.C., 2007. Carbon-isotope record of the Early Jurassic (Toarcian) Oceanic Anoxic Event from fossil wood and marine carbonate (Lusitanian Basin, Portugal). Earth Planet. Sci. Lett. 253 (3–4), 455–470.
Hesselbo, S.P., 2008. Sequence stratigraphy and inferred relative sea-level change from the onshore British Jurassic. Proceedings of the Geologists' Association 119, 19–34.
Howarth, M.K., 1956. The Scalpa Sandstone of the Isle of Raasay. Proceedings of the Yorkshire Geological Society 30, 353–370.
Howarth, M.K., 1992. The ammonite family Hildoceratidae in the Lower Jurassic of Britain. Monograph of the Palaeontographical Society 145, 1–106.
Ikeda, M., Hori, R.S., Ikehara, M., Miyashita, R., Chino, M., Yamada, K., 2018. Carbon cycle dynamics linked with Karoo-Ferrar volcanism and astronomical cycles during Pliensbachian-Toarcian (Early Jurassic). Glob. Planet. Chang. 170, 163–171.
Izumi, K., Kemp, D.B., Itamiya, S., Inui, M., 2018a. Sedimentary evidence for

enhanced hydrological cycling in response to rapid carbon release during the early Toarcian oceanic anoxic event. Earth Planet. Sci. Lett. 481, 162–170.

Izumi, K., Endo, K., Kemp, D.B., Inui, M., 2018b. Oceanic redox conditions through the late Pliensbachian to early Toarcian on the northwestern Panthalassa margin: Insights from pyrite and geochemical data. Palaeogeogr. Palaeoclimatol. Palaeoecol. 493, 1–10.

Jenkyns, H.C., 1988. The early Toarcian (Jurassic) anoxic event-stratigraphic, sedimentary, and geochemical evidence. Am. J. Sci. 288 (2), 101–151.

Kemp, D.B., Coe, A.L., Cohen, A.S., Schwark, L., 2005. Astronomical pacing of methane release in the Early Jurassic period. Nature 437 (7057), 396–399.

Kemp, D.B., Izumi, K., 2014. Multiproxy geochemical analysis of a Panthalassic margin record of the early Toarcian oceanic anoxic event (Toyora area, Japan). Palaeogeogr. Palaeoclimatol. Palaeoecol. 414, 332–341.

Kemp, D.B., Baranyi, V., Izumi, K., Burgess, R.D., 2019. Organic matter variations and links to climate change across the early Toarcian oceanic anoxic event (T-OAE) in Toyora area, southwest Japan. Palaeogeogr. Palaeoclimatol. Palaeoecol. 530, 90–102.

Kemp, D.B., Selby, D., Izumi, K., 2020. Direct coupling between carbon release and weathering during the Toarcian oceanic anoxic event. Geology 48, 976–980.

Korty, R.L., Emanuel, K.A., Huber, M., Zamora, R.A., 2017. Tropical cyclones down-scaled from simulations with very high carbon dioxide levels. J. Climate 30 (2), 649–667.

Krencker, F.N., Bodin, S., Suan, G., Heimhofer, U., Kabiri, L., Immenhauser, A., 2015. Toarcian extreme warmth led to tropical cyclone intensification. Earth Planet. Sci. Lett. 425, 120–130.

Lee, G.W., 1920. The Mesozoic Rocks of Applecross, Raasay and North-East Skye (with Contributions and Appendix by S.S. Buckman), Memoir of the Geological Survey of Great Britain, sheets 81 and 71 (Scotland), HMSO, Edinburgh, 93 pp.

Little, C.T.S. 1995. The Pliensbachian–Toarcian (Lower Jurassic) extinction event. PhD thesis, Bristol University.

Liu, D., Huang, C., Ogg, J.G, Kemp, D.B., li, M., Yu, M., Foster, W.J., 2021. Astronomically forced changes in chemical weathering and redox during the Anisian (Middle Triassic): Implications for marine ecosystem recovery following the end-Permian mass extinction. Palaeogeogr. Palaeoclimatol. Palaeoecol. 569, 110355.

Masselink, G., van Heteren, S., 2014. Response of wave-dominated and mixed-energy barriers to storms. Mar. Geol. 352, 321–347.

McArthur, J.M., Algeo, T.J., van de Schootbrugge, B., Li, Q., Howarth, R.J., 2008. Basinal restriction, black shales, Re-Os dating, and the Early Toarcian (Jurassic) oceanic anoxic event. Paleoceanography 23 (4), PA4217.

McElwain, J.C., Wade-Murphy, J., Hesselbo, S.P., 2005. Changes in carbon dioxide during an oceanic anoxic event linked to intrusion into Gondwana coals. Nature 435 (7041), 479–482.

Meyers, P.A., 1997. Organic geochemical proxies of paleoceanographic, palaeolimnologic, and paleoclimatologic processes. Org. Geochem. 27, 213–250.

Morton, N., 1989. Jurassic sequence stratigraphy in the Hebrides Basin, NW Scotland. Marine and Petroleum Geology 6, 243–260.

Morton, N., Hudson, J.D., 1995. Field guide to the Jurassic of the Isles of Raasay and Skye, Inner Hebrides, NW Scotland. In Field Geology of the British Jurassic (ed. P.D. Taylor), Geological Society, London 209–280.

Morton, N., 2009. Cadha Carnach, Isle of Raasay, Highlands. Geological Conservation Review Series British Lower Jurassic Stratigraphy.

Pearce, C.R., Cohen, A.S., Coe, A.L., Burton, K.W., 2008. Molybdenum isotope evidence for global ocean anoxia coupled with perturbations to the carbon cycle during the early jurassic. Geology 36 (3), 231–234.

Percival, L.M.E., Cohen, A.S., Davies, M.K., Dickson, A.J., Hesselbo, S.P., Jenkyns, H.C., Leng, M.J., Mather, T.A., Storm, M.S., Xu, W., 2016. Osmium isotope evidence for two pulses of increased continental weathering linked to Early Jurassic volcanism and climate change. Geology 44 (9), 759–762.

Price, G.D., 2010. Carbon-isotope stratigraphy and temperature change during the Early–Middle Jurassic (Toarcian–Aalenian), Raasay, Scotland, UK. Palaeogeogr. Palaeoclimatol. Palaeoecol. 285 (3–4), 255–263.

Remirez, M., Algeo, T.J., 2020a. Carbon-cycle changes during the Toarcian (Early Jurassic) and implications for regional versus global drivers of the Toarcian oceanic anoxic event. Earth Sci. Rev. 209, 103283.

Remirez, M., Algeo, T.J., 2020b. Paleosalinity proxy evidence for watermass restriction in the Cleveland Basin (UK) during the Toarcian OAE. Earth Sci. Rev. 201, 103072.

Roberts, A.M., Holdsworth, R.E., 1999. Linking onshore and offshore structures: Mesozoic extension in the Scottish Highlands. Journal of the Geological Society, London 156, 1061–1064.

Ruebsam, W., Reolid, M., Sabatino, N., Masetti, D., Schwark, L., 2020. Molecular paleothermometry of the early Toarcian climate perturbation. Glob. Planet. Chang. 195, 103351.

Ruvalcaba Baroni, I., Pohl, A., van Helmond, N.A.G. M., Papadomanolaki, N.M., Coe, A.L., Cohen, A.S., van de Schootbrugge, B., Donnadieu, Y., Slomp, C.P., 2018. Ocean circulation in the Toarcian (Early Jurassic), a key control on deoxygenation and carbon burial on the European Shelf. Paleoceanography and Paleoclimatology 33 (9), 994–1012.

Scholz, F., 2018. Identifying oxygen minimum zone-type biogeochemical cycling in Earth history using inorganic geochemical proxies. Earth Sci. Rev. 184, 29–45.

Schouten, S., Kaam-Peters, H. M.E.V., Schoell, M., Sinninghe-Damste, J.S., 2000. Effects of an oceanic anoxic event on the stable carbon isotopic composition of early Toarcian carbon. American Journal of Science 300 (1), 1–22.

Slater, S.M., Twitchett, R.J., Danise, S., Vajda, V., 2019. Substantial vegetation response to Early Jurassic global warming with impacts on oceanic anoxia. Nat. Geosci. 12, 462–467.

Stein, A., 1988. Basement controls upon basin development in the Caledonian foreland,

NW Scotland. Basin Research 1, 107–119.
Suan, G., Pittet, B., Bour, I., Mattioli, E., Duarte, L.V., Mailliot, S., 2008. Duration of the Early Toarcian carbon isotope excursion deduced from spectral analysis: consequence for its possible causes. Earth Planet. Sci. Lett. 267 (3–4), 666–679.
Suan, G., Van De Schootbrugge, B., Adatte, T., Fiebig, J., Oschmann, W., 2015. Calibrating the magnitude of the Toarcian carbon cycle perturbation. Paleoceanography 30 (5), 495–509.
Svensen, H., Planke, S., Chevallier, L., Malthe-Sorenssen, A., Corfu, F., Jamtveit, B., 2007. Hydrothermal venting of greenhouse gases triggering Early Jurassic global warming. Earth Planet. Sci. Lett. 256 (3–4), 554–566.
Tankard, A.J., Balkwill, H.R., 1989. Extensional tectonics and Stratigraphy of the North Atlantic Margins. American Association of Petroleum Geologists, Memoirs 46.
Taylor, S.R., McLennan, S.M., 1985. The Continental Crust: Its Composition and Evolution. Blackwell, Malden, Mass.
Them, T.R., Gill, B.C., Caruthers, A.H., Grocke, D.R., Tulsky, E.T., Martindale, R.C., Poulton, T.P., Smith, P.L., 2017. High-resolution carbon isotope records of the Toarcian Oceanic Anoxic Event (Early Jurassic) from North America and implications for the global drivers of the Toarcian carbon cycle. Earth Planet. Sci. Lett. 459, 118–126.
Thibault, N., Ruhl, M., Ullmann, C.V., Korte, C., Kemp, D.B., Grocke, D.R., Hesselbo, S.P., 2018. The wider context of the Lower Jurassic Toarcian oceanic anoxic event in Yorkshire coastal outcrops, UK. Proc. Geol. Assoc. 129 (3), 372–391.
Thierry, J., 2000. Middle Toarcian, map. 8. In: Dercourt, J., Gaetani, M., Vrielynck, B., Barrier, E., Biju-Duval, B., Brunet, M.F. ... Sandulescu, M. (Eds.), Altlas Peri-Tethys Palaeogeographical Maps. CCGM/CGMW, Paris, pp. 61–70.
Tribovillard, N., Algeo, T.J., Lyons, T., Riboulleau, A., 2006. Trace metals as paleoredox and paleoproductivity proxies: an update. Chem. Geol. 232 (1–2), 12–32.
Tribovillard, N., Algeo, T.J., Baudin, F., Riboulleau, A., 2012. Analysis of marine environmental conditions based on molybdenum–uranium covariation—Applications to Mesozoic paleoceanography. Chem. Geol. 324–325, 45–58.
van Krevelen, D.W., 1981. In: Van Krevelen, D.W. (Ed.), Coal Science and Technology. Coal, Elsevier, Amsterdam, pp. 129–314.Wang, Y., Ossa, F.O., Spangenberg, J.E., Wille, M., et al., 2021. Restricted oxygen-deficient basins on the Northern European epicontinental shelf across the Toarcian carbon isotope excursion interval. Paleoceanography and Paleoclimatology 36, e2020PA004207.
Wignall, P.B., 1994. Black Shales, 127 pp., Clarendon, Oxford, UK.
Xu, W., Ruhl, M., Jenkyns, H.C., Hesselbo, S.P., Riding, J.B., Selby, D., Naafs, B.D.A., Weijers, J.W.H., Pancost, R.D., Tegelaar, E.W., Idiz, E.F., 2017. Carbon sequestration in an expanded lake system during the Toarcian oceanic anoxic event. Nat. Geosci. 10 (2), 129–134.
Xu, W., Ruhl, M., Jenkyns, H.C., et al., 2018. Evolution of the Toarcian (Early Jurassic) carbon-cycle and global climatic controls on local sedimentary processes

(Cardigan Bay Basin, UK). Earth Planet. Sci. Lett. 484, 396–411.

Figures

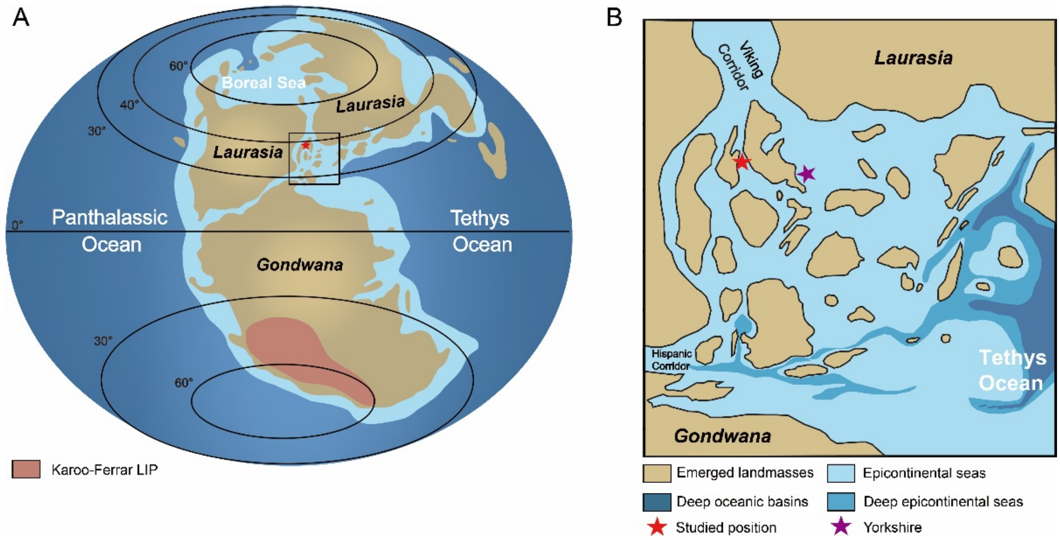

Fig. 1. (A) Global Toarcian paleogeographic reconstruction with the location of the Karoo-Ferrar Large Igneous Province (shaded red) in southern Gondwana (after Dera et al., 2009), and the location of the Raasay section (red star). (B) Detailed paleogeographic map of the Northwest European Shelf (NWES) and western Tethys (after Thierry, 2000), with the locations of the Raasay section (Hebrides Basin, red star) and nearby Yorkshire section (Cleveland Basin, purple star) also shown.

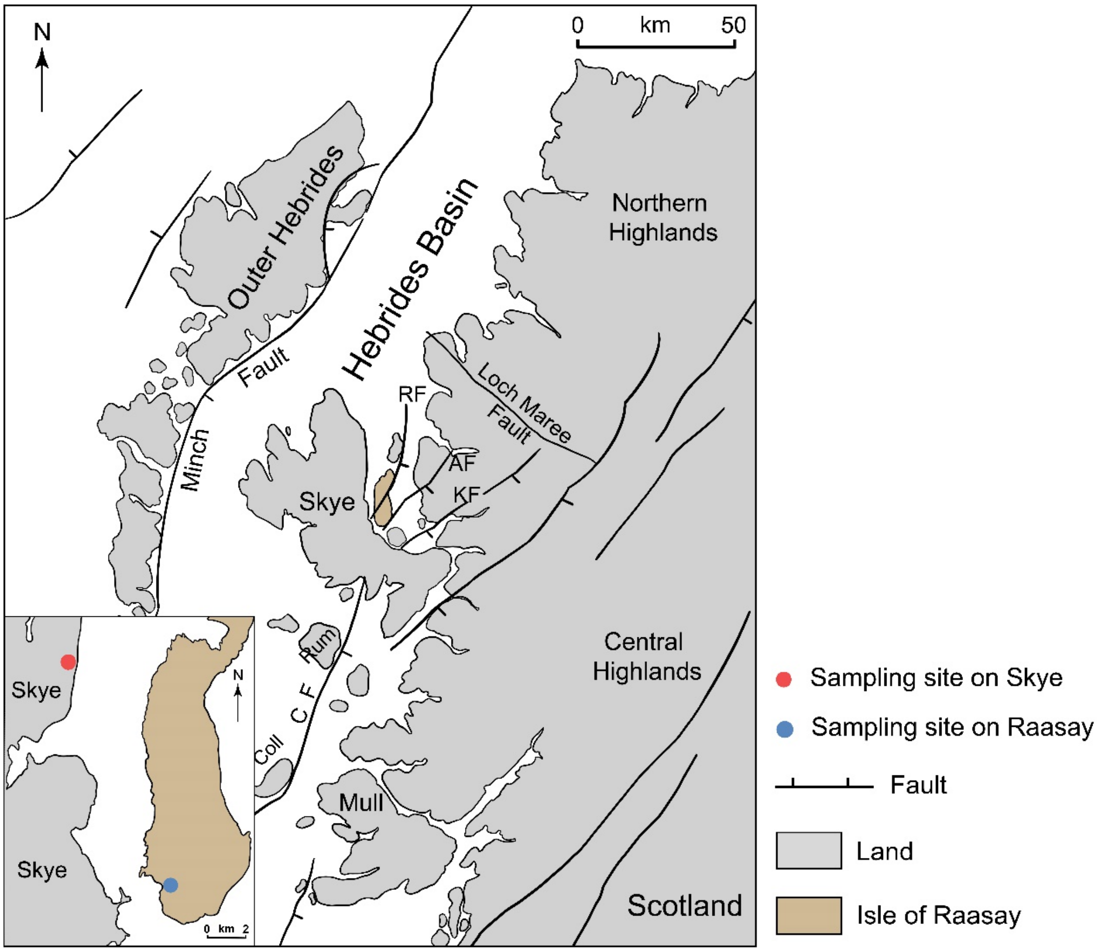

Fig. 2. Simplified map of Hebrides Basin (after Roberts and Holdsworth, 1999). Abbreviations: AF, Applecross Fault; CF, Camasunary Fault; RF, Raasay Fault; KF, Kishorn fault. The red dot shows the location of the sampling site on Skye and the blue dot shows the location of the sampling site on Raasay.

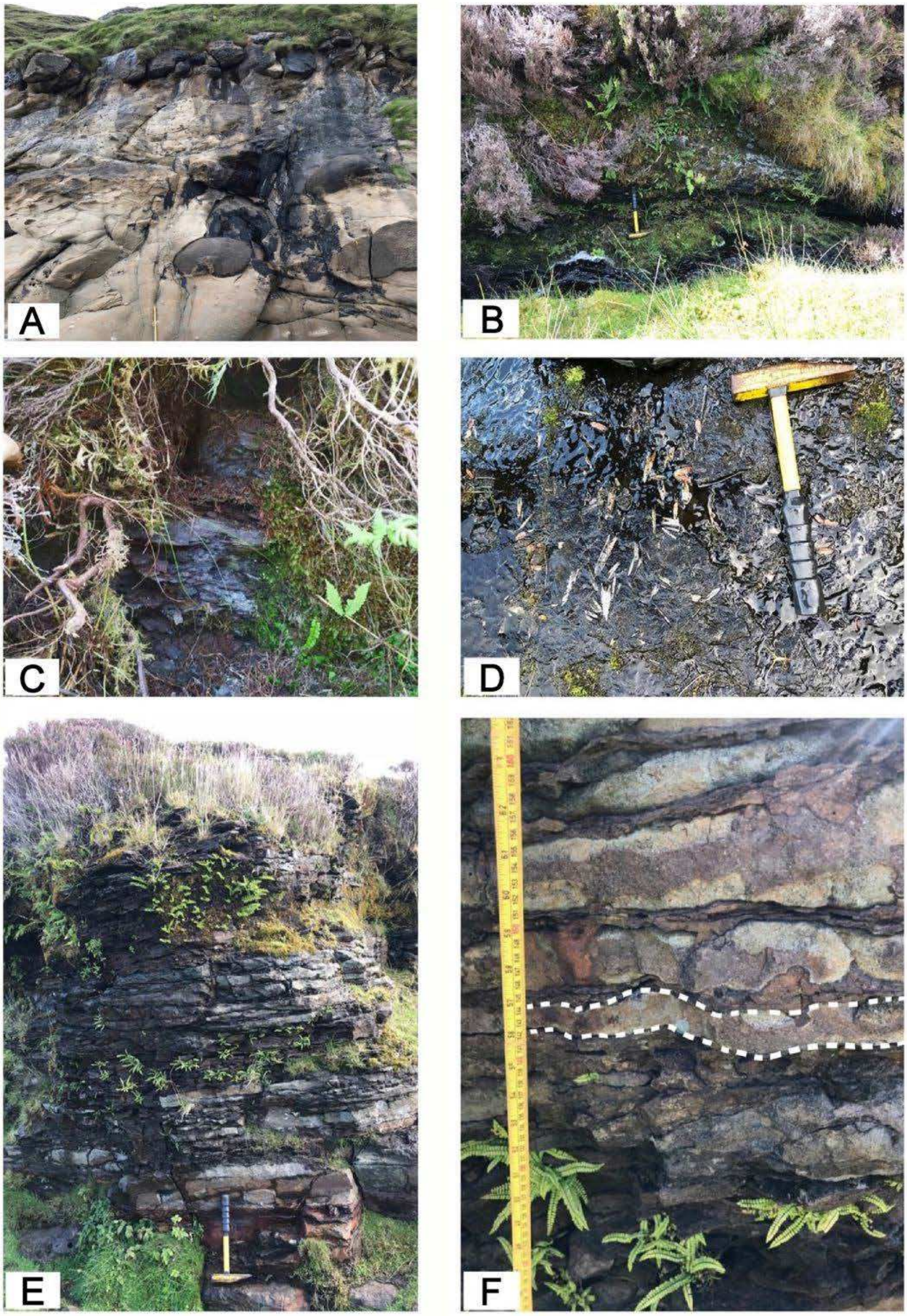

Fig. 3. Field photographs of the Skye and Raasay sections. (A) top of the Scalpa Sandstone Formation exposed on the east coast of Skye (NG 5156 4710) (top 50 cm of ruler is visible at base of the image). (B) Portree Shale Formation outcrop in Inverarish Burn (NG 5719 3688) (exposed section thickness is ~60 cm in this image). The top of the Scalpa Sandstone Formation is hidden in the stream ~40 cm below the hammer. (C)

Portree Shale Formation at Inverarish Burn, characterized by fissile dark shales. (D) “Belemnite battlefield” marking the top of the Portree Shale Formation, exposed nearby Inverarish Burn. (E) Raasay Ironstone Formation exposed in the area of the main opencast ironstone workings (NG 5690 3645). (F) Unevenly bedded ironstones intercalated with mudstones (white dashed lines highlight bed boundaries).

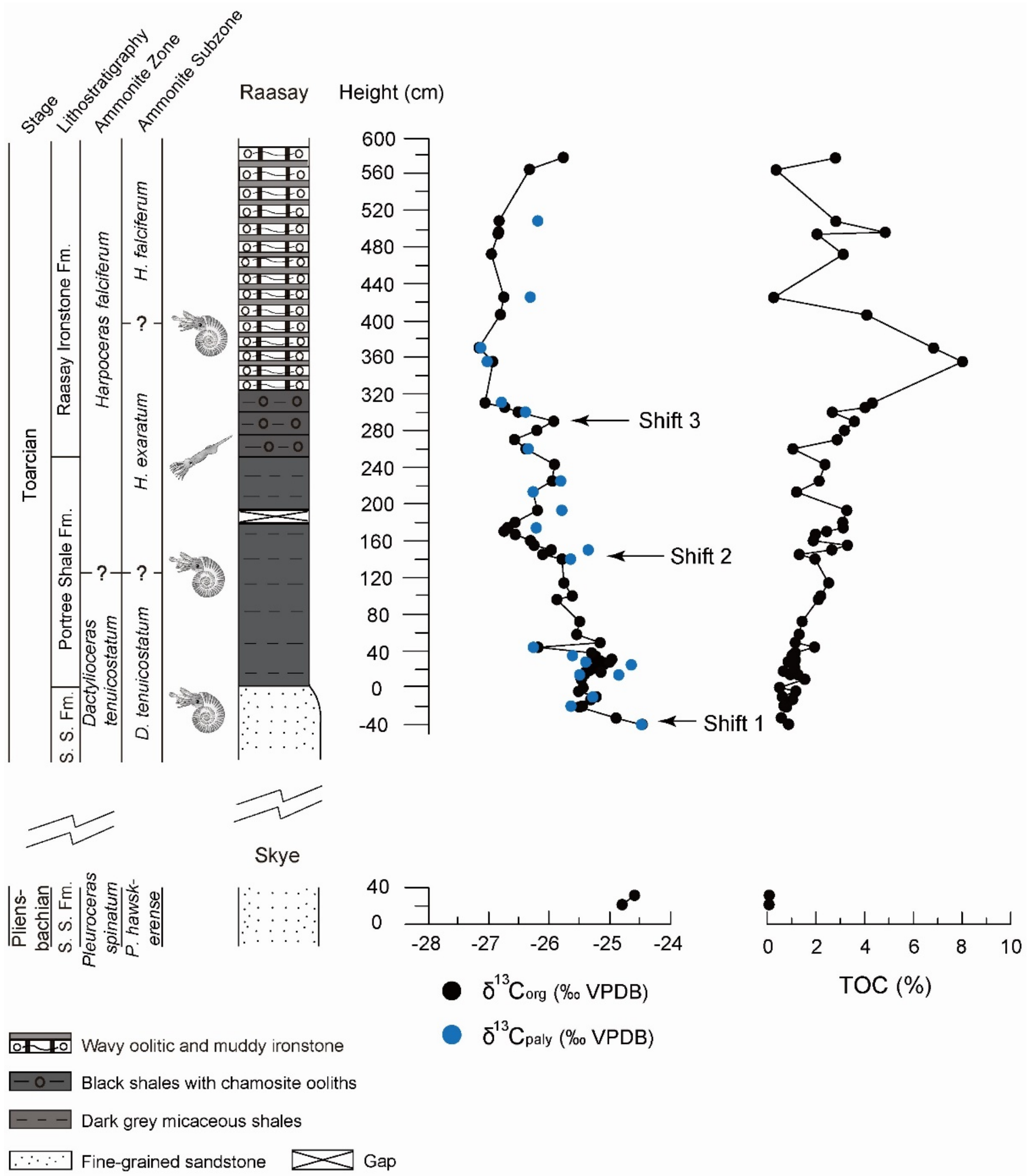

Fig. 4. Litho- and bio-stratigraphy, bulk organic carbon isotope ($\delta^{13}C_{org}$), palynological carbon isotope ($\delta^{13}C_{paly}$) and total organic carbon (TOC) data from the uppermost Pliensbachian to Toarcian from the Skye and Raasay sections. Bedding in the ironstone is shown schematically, but at the correct general scale. Fossil images indicate horizons with observed enrichment. Biostratigraphy of the sections is derived from Lee (1920), Howarth (1956, 1992) and Morton and Hudson (1995) (see Section 2.2 for details). Fm. = Formation. S. S. = Scalpa Sandstone

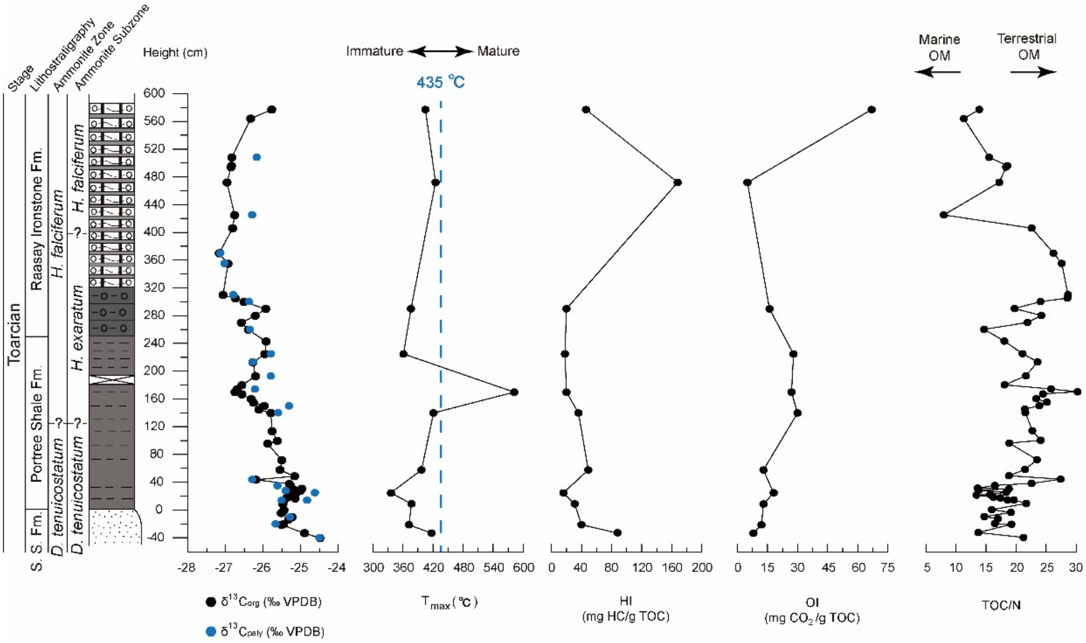

Fig. 5. Carbon isotope, Rock Eval, and TOC/N data through the Raasay section. The blue vertical dashed line denotes the threshold of the oil window for Type III kerogen. See main text for details. OM = organic matter.

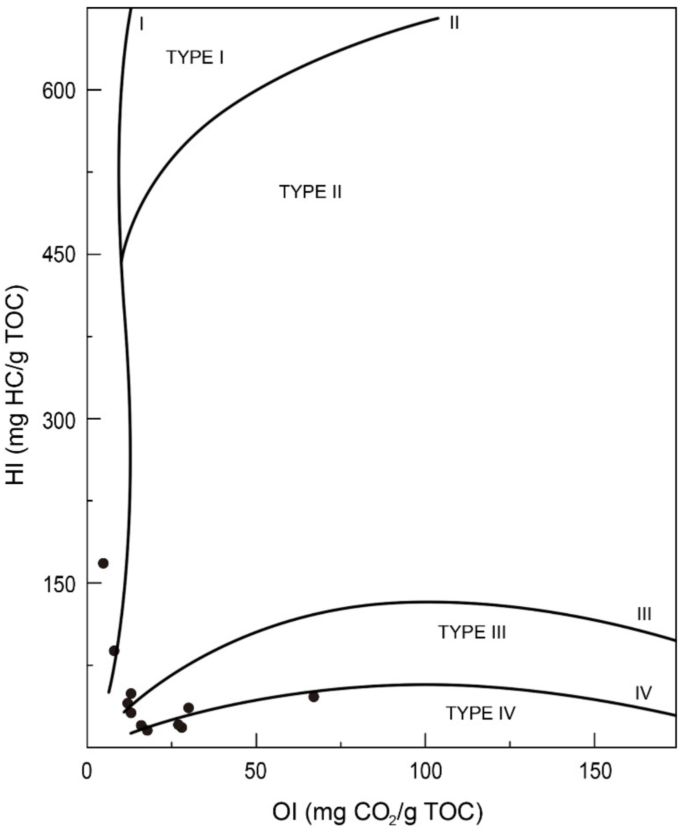

Fig. 6. Cross plot (van Krevelen diagram) of HI versus OI from Rock Eval measurements of the Raasay samples. The plot indicates that the Raasay samples are mainly composed of type III to type IV organic matter, of likely terrestrial origin.

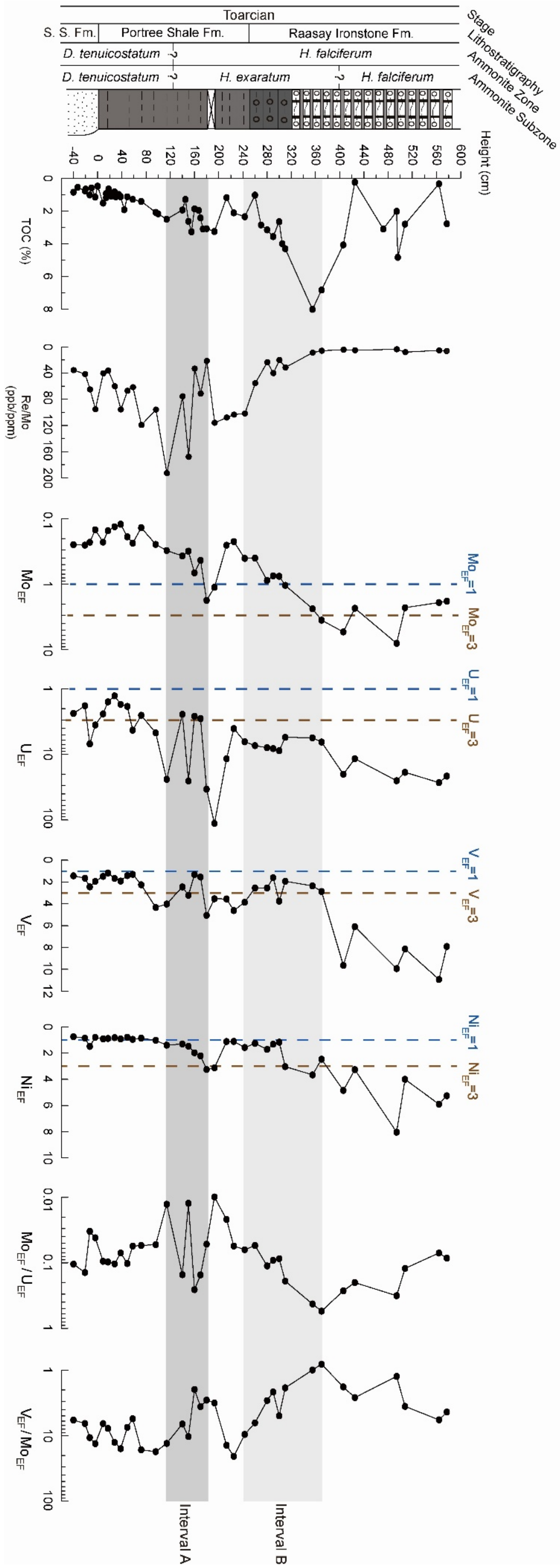

Toarcian
Stage
Lithostratigraphy
Ammonite Zone
Ammonite Subzone
S. S. Fm.
Portree Shale Fm.
Raasay Ironstone Fm.
D. tenuicostatum
H. falciferum
H. exaratum
Height (cm)
TOC (%)
Re/Mo (ppb/ppm)
Mo_{EF}
Mo_{EF}=1
Mo_{EF}=3
U_{EF}
U_{EF}=1
U_{EF}=3
V_{EF}
V_{EF}=1
V_{EF}=3
Ni_{EF}
Ni_{EF}=1
Ni_{EF}=3
Mo_{EF} / U_{EF}
V_{EF} / Mo_{EF}
Interval A
Interval B

Fig. 7. Total organic carbon (TOC) and redox-sensitive proxies (Mo_{EF}, U_{EF}, V_{EF}, Ni_{EF}, Re/Mo, Mo_{EF}/U_{EF}, and V_{EF}/Mo_{EF}) through the Raasay section. Note that Mo_{EF}, U_{EF}, Mo_{EF}/U_{EF} and V_{EF}/Mo_{EF} are shown on logarithmic scales. The blue dashed line (X_{EF}=1) represents the boundary of enrichment versus depletion, and the brown dashed line (X_{EF}=3) represents 'detectable' enrichment (see main text for details). The shaded intervals indicate the relative enrichment of Mo compared to U and V based on changes in Mo_{EF}/U_{EF} and V_{EF}/Mo_{EF} ratios (see main text for details).

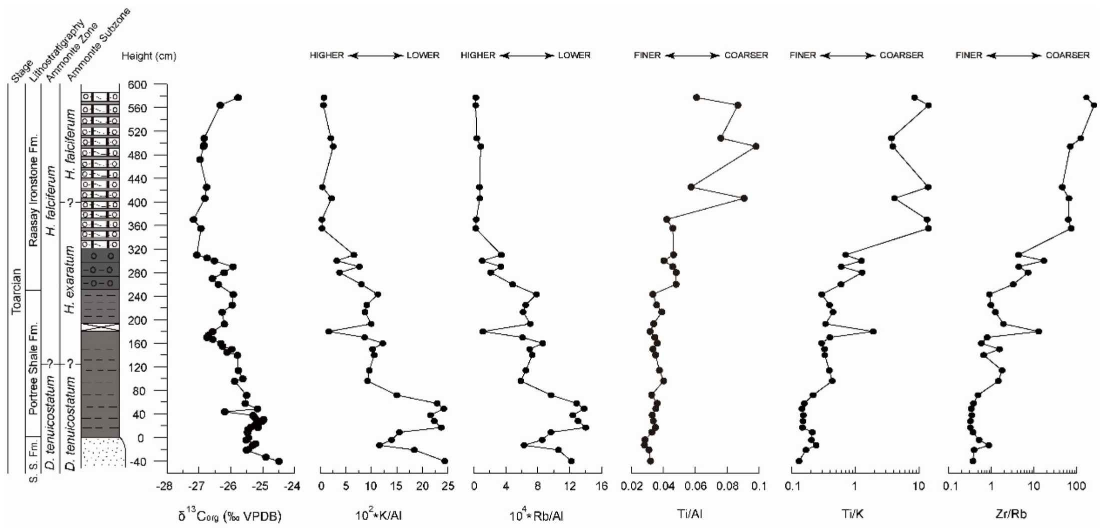

Fig. 8. Carbon isotope ($\delta^{13}C_{org}$) data, chemical weathering proxies (K/Al and Rb/Al), and detrital proxies (Ti/Al, Ti/K and Zr/Rb) through the Raasay section. The horizontal arrows above the figures denote the inferred variations in chemical weathering rate (higher versus lower) and grain sizes (finer versus coarser). Note the logarithmic scales for Ti/K and Zr/Rb.

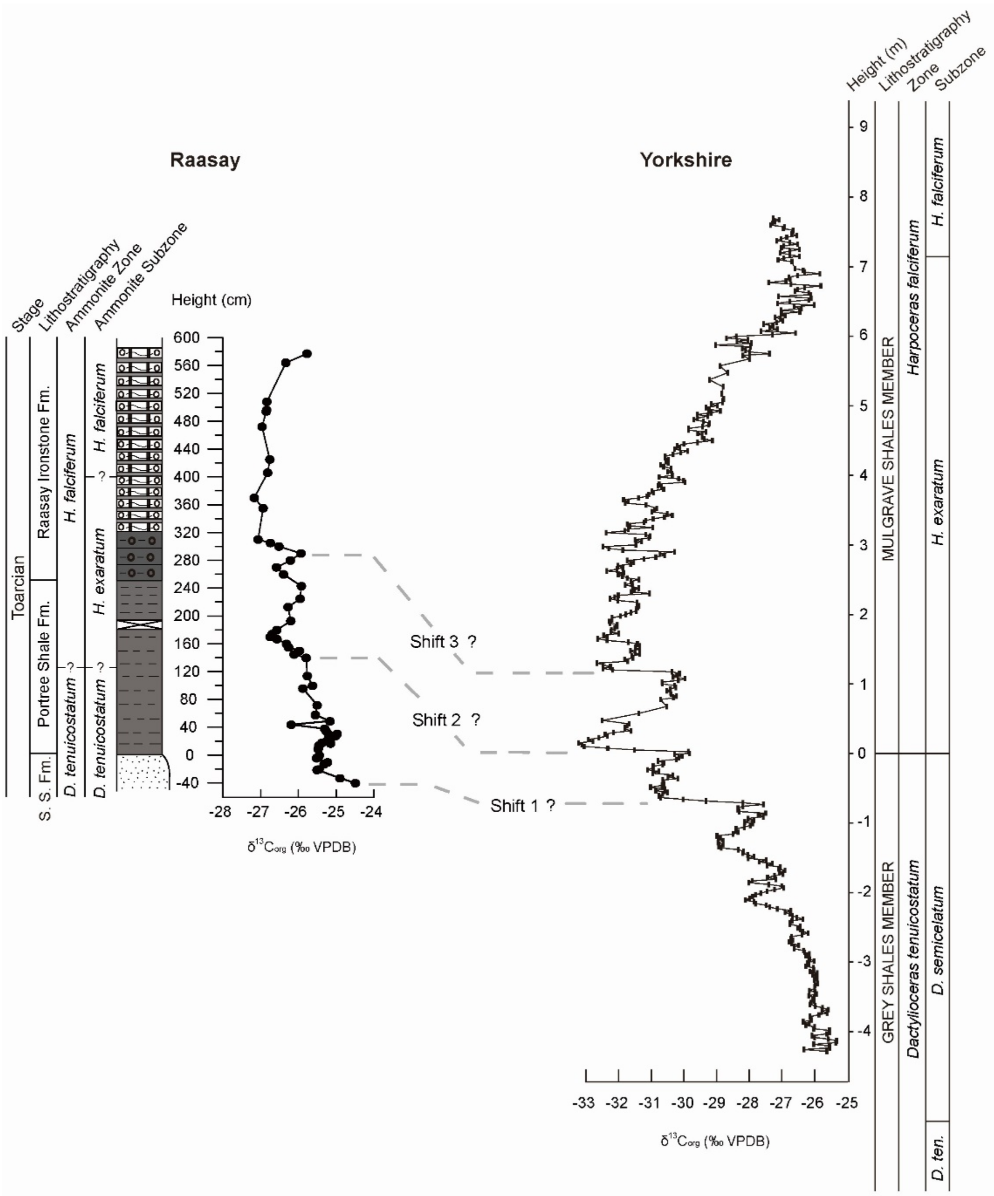

Fig. 9. Suggested carbon isotope correlation between the Raasay section (this study) and the Yorkshire section, Cleveland Basin (Yorkshire data from Kemp et al., 2005). The $\delta^{13}C_{org}$ profiles in these two sections exhibit generally similar trends, characterized by a pronounced negative trend and subsequent positive recovery. The profiles have been tentatively correlated (grey dashed lines) based on the presence of three abrupt shifts in each section, which is also consistent with the available biostratigraphy. ten. = tenuicostatum.

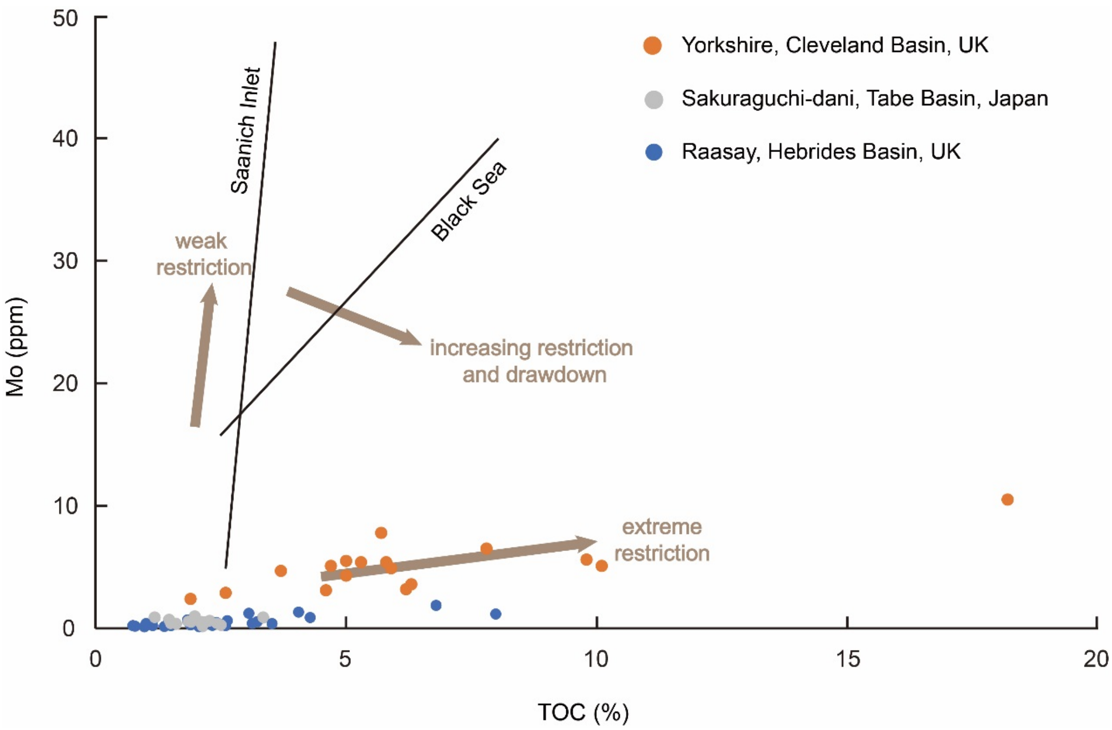

Fig. 10. Cross plot of Mo and TOC from Raasay (this study), Yorkshire (Cleveland Basin, UK; McArthur et al., 2008), and Sakuraguchi-dani (Tabe Basin, Japan; Kemp and Izumi, 2014) within the T-OAE interval of each section. This plot can be used to interpret either the degree of water mass restriction in oxygen-limited marine basins (in the case of the Cleveland Basin), or a lack of appreciable Mo enrichment in oxygenated settings (in the case of the Tabe and Hebrides Basin). The black solid lines show the trends in two modern basins characterized by watermass restriction (see also Algeo and Lyons, 2006). See main text for discussion.